Journal of Materials Science manuscript No.
(will be inserted by the editor)

Analytical solution for multi-component pyrolysis simulations of thermal protection materials

Joffrey Coheur · Francisco Torres-Herrador · Philippe Chatelain · Nagi N. Mansour · Thierry E. Magin · Maarten Arnst

Received: date / Accepted: date

Abstract This paper provides the analytical solution to a one-parameter Šesták-Berggren kinetic model for the thermoanalytical study of pyrolysis reactions involving multiple independent parallel reactions. Such multiple independent parallel reactions are widely used, for instance, in the modeling of the pyrolysis of thermal protection materials used in heatshields for spacecraft during the atmospheric entry phase. Solving inverse problems to infer parameters of the kinetic model through optimization techniques or Bayesian inference methods for uncertainty quantification may require a large number of evaluations of the response and its sensitivities (derivatives with respect to parameters). Moreover, in the case of kinetic equations, the Arrhenius parameters can exhibit strong dependence that can require further model evaluations for an accurate parameter calibration. The interest of this analytical solution is to reduce computation cost while having high accuracy to perform parameter calibration from experiments and sensitivity analysis. We propose to use exponential-integral functions to express the solution of the temperature integral and we derive the analytical solution and its sensitivities for the parallel reaction model both for constant temperature (isothermal) and for constant heating rate conditions. The solution is validated on a six-equation model using parameters inferred in a previous work from the experimental data of the pyrolysis of a phenolic-impregnated carbon ablator (PICA)

J. Coheur · M. Arnst
Université de Liège, Aerospace and Mechanical Engineering, Allée de la Découverte 9, 4000 Liège, Belgium
Tel.: +32-474-464-030
E-mail: joffrey.coheur@uliege.be

J. Coheur · F. Torres-Herrador · Thierry E. Magin
von Karman Institute for Fluid Dynamics, 1640 Rhode-St-Genèse, Belgium

J. Coheur · P. Chatelain
Institute of Mechanics, Materials and Civil Engineering (iMMC), Université catholique de Louvain, Place du Levant 2, 1348 Louvain-la-Neuve, Belgium

N. N. Mansour
NASA Ames Research Center, CA 94035 Moffett Field, USA

material, and we compare the computational cost and accuracy of the implemented analytical solution with a numerical solution. Our results show that the use of such analytical solution with an accurate computation of the exponential-integral function significantly reduces the computational cost compared to the numerical solution.

Keywords Multi-step kinetics · Temperature integral · Exponential-integral · Analytical solution · Pyrolysis · Thermal protection materials · Arrhenius equation · Sensitivity analysis

1 Introduction

During the atmospheric entry of spacecraft, the high temperatures achieved ($> 4\,000\,\mathrm{K}$) cannot be withstood by any known material [1]. A successful solution for shielding spacecraft is the use of carbon/phenolic ablative thermal protection materials (TPMs) [2–7]. These materials undergo physico-chemical transformations by which they absorb part of the incoming heat while getting decomposed. One of the main endothermic processes is the pyrolysis of the phenolic phase of the composite.

Thermoanalytical studies involve using experiments to determine the reaction process provided a given temperature increase and characterize the species that are produced through the reaction. For instance, in order to study the pyrolysis decomposition of TPMs and in particular porous carbon/phenolic composites, recent experimental studies have been reported in Wong et al. [8,9] and Bessire et al. and Torres-Herrador et al. [10,11], in which the pyrolysis was carried out under isothermal conditions and linearly increasing temperature, respectively. The mass of the sample as a function of temperature and for different heating rates is typically monitored using thermogravimetric analysis (TGA), such as in [8,9,11]. Furthermore, in Bessire et al. [10], the identification and production of the volatile decomposition products are measured by a mass spectrometer, while in Wong et al. [8,9] they are measured using gas chromatography techniques.

A widely used formulation for the pyrolysis of TPMs is the multi-component (or multi-step) pyrolysis model [12–17]. When the material is heated, it is decomposed following independent reaction processes that occur in parallel, each of them representing the decomposition of a sub-phase, or component, in the solid. The use of multi-component models for pyrolysis is not limited to the application to TPMs. They are also widely used in fire safety [18–25] or (less commonly) in biomass [17].

The reaction rate characterizing the reaction processes are usually parametrized in terms of temperature and the extent of conversion (or advancement of reaction factor). The dependence on temperature, called the rate constant, is typically parameterized through the Arrhenius equation. The dependence on the extent of conversion is parameterized using a model reaction that depends on the type of the reaction [26]. In particular, the majority of model reactions can be generalized using the Šesták-Berggren equation [27–29]. One of the objectives of kinetic studies is to determine the kinetic parameters appearing in the parameterization of the rate constant and the model reaction.

However, in general, the reaction rates cannot be measured directly and one must solve an inverse problem in order to infer the kinetic parameters. Several methods

have been used in order to infer kinetic parameters (see reviews in [30–32]). Model-free approaches allow to evaluate the activation energy without the need of providing the model reaction. The isoconversional method is the most common model-free method and relies on the isoconversional principle that states that the reaction rate is only a function of the temperature at a fixed value of the extent of conversion. A variant of the isoconversional method is the integral isoconversional method, used to improve the accuracy of the method, and is obtained by integrating the reaction rate and applying to it the isoconversional principle. The integration of the rate constant over the temperature range is termed the temperature-integral (or Arrhenius integral) and its solution has been extensively studied, as discussed below.

When the reaction process is complex, e.g. competitive reaction or multi-component reactions, and cannot be expressed in terms of one-step kinetics, one generally resorts to model-fitting approaches. Model-fitting approaches allow to infer at the same time kinetic parameters and to postulate the model reaction. They consist in formulating the inverse problem, for instance, as an optimization problem that seeks to minimize the mismatch between the experimental observations and the model representing the physics. This mismatch can be expressed as the sum of the squares of the residuals between the experimental observations and the output of the model given its parameter values [33,16]. In a Bayesian framework, this mismatch can appear in the argument of a likelihood function in a Bayes formula [34,35]. In both cases, the solution of this inverse problem is usually performed numerically and requires the repeated computation of the model output for given parameters that can be computationally expensive, in particular when computations of derivatives with respect to the parameters are needed. Moreover, in the case of kinetic equations, the Arrhenius parameters inferred from model-fitting approaches can exhibit strong dependence, known as the kinetic compensation effect [36,26,31], and can require even further model evaluations for an accurate parameter calibration. Comparisons of model-free and model-fitting methods are provided for instance in [33,37,31]. Therefore, having an efficient—analytical—computation of the solution is convenient when a large number of model evaluations is required.

For both the model-free and the model-fitting methods, the computation of the temperature integral is required. The class of model-free methods has been the subject of many studies for solving the temperature integral. The main challenge in the calculation of the analytical solution is in finding the expression of the temperature integral, which solution depends on the temperature program of the experiment. In the case of a linearly increasing temperature, this temperature integral can be expressed in terms of special functions and in particular an exponential integral function [38–40]. In thermoanalytical studies, exponential integral functions can be evaluated by using various approximation formulae [41–43,40,31] or by computing the integral numerically [44]. The approximation formulae can result in different approximate values of the temperature integral with different levels of accuracy, sometimes resulting in discrepancies in the activation energy [43,40]. With the improvement of computational resources, Orfao [45] suggested that numerical integration should be used whenever it is possible.

Nowadays, the computational power and the efficient implementation in software packages of the special functions appearing in the analytical solution of the tempera-

ture integral allow an accurate computation of their values in an amount of time comparable to the evaluation of approximation formulae or their numerical integration. Recently, Carrero and Rojas [46] performed a comparison of the numerical integration using a Simpson 3/8 rule of the temperature integral with its solution including different implementations of the special functions. The authors showed that the relative errors between the numerical integration and the solutions with the exponential integral were of the order of 10^{-10}. This makes the use of the analytical solution of the temperature integral both accurate and computationally efficient.

Therefore, the main contributions of this paper are the followings. We obtain the analytical solution and its derivatives with respect to kinetic parameters (sensitivities) for multi-step (or multicomponent) reactions featuring a one-parameter Šesták-Berggren reaction model. As in [46], we provide the derivation of the analytical solution of the temperature integral based on an accurate and fast computation of the exponential-integral function. We illustrate the computational gain and accuracy that is achieved by using this analytical expression compared to a numerical solution of the initial value problem that models the reaction.

As an illustration, we apply the analytical solution to the multicomponent model to the pyrolysis of TPMs from the experiment of Bessire et al. [10] for which the kinetic parameters were inferred in Torres-Herrador et al. [16] on a single heating rate. However, other applications in which the heating rate varies can also benefit from the analytical solution such as in Bruns [22], for the pyrolysis of high-impact polystyrene, bisphenol-A polycarbonate and polyvinyl chloride and where the kinetic parameters are calibrated separately at 3 and 10 $\mathrm{K\,min^{-1}}$; in Yuen et al. [24,23] for the pyrolysis of flexible polyurethane at the heating rates 10, 20, and 35 $\mathrm{K\,min^{-1}}$and for which the same kinetic parameters are found for the multi-component model; or in Torres-Herrador et al. [17] for the pyrolysis of lignocellulosic biomass at 5, 20 and 40 $\mathrm{K\,min^{-1}}$again with the same kinetic parameters.

The paper is organized as follows. In Sect. 2.1, we review the modeling of pyrolysis by using in a set of independent parallel reactions and establish the conditions in which we are interested. Then, in Sect. 2.2, we derive the analytical solution to the system of differential equations along with its gradient with respect to model parameters. In Sect. 3, we present the material considered for the pyrolysis simulations, the experimental set-up and the calibration method for material properties are briefly recalled. Finally, in Sect. 4, we verify the accuracy and computational speed of the implemented analytical solution by comparing it with the numerical solution for a six-reaction pyrolysis model that was fitted previously to a non-isothermal experiment and we perform a local sensitivity analysis.

2 Analysis

2.1 Mathematical description of multi-component pyrolysis

The literature on pyrolysis of organic compounds is vast [26,30,31], and many different models have been proposed to simulate this process. In this work, we focus on multi-component (parallel) models since they are the most used in aerospace en-

gineering for modeling thermal protection material decomposition [13,16]. These models assume that the pyrolysing solid is made up of different sub-phases which independently undergo pyrolysis. We first start with a short review of the single-stage kinetic equation and the parameterization for the constant rate and model reaction. We then explain the multi-stage pyrolysis model.

2.1.1 Single-stage kinetic equation

A pyrolysis reaction occurs when an organic compound is submitted to high temperatures in the absence of oxygen. This reaction is typically assumed to be a non-reversible process whose evolution is governed by a reaction rate. In this process, the reactant R gets decomposed into different gaseous products S_j, with $1 \leq j \leq N_\mathrm{s}$ and N_s the total number of species, and a residual solid known as char (denoted C)

$$\mathrm{R}^{(s)} \xrightarrow{k} \mathrm{C}^{(s)} + \gamma_1 \mathrm{S}_1^{(g)} + \gamma_2 \mathrm{S}_2^{(g)} + \cdots + \gamma_j \mathrm{S}_j^{(g)}, \tag{1}$$

where the γ_j are the stoichiometric coefficients and the superscripts denote the state of matter, either solid (s) or gaseous (g) here.

It is common to describe the amount of decomposition which has taken place using the dimensionless fractional decomposition factor $\alpha(t)$ (or advancement of reaction factor, or extent of reaction, or extent of conversion) as a function of time. Here, we will take this factor as varying from 0 for the virgin reactant to 1 signifying the complete decomposition. This factor is related to the mass $m(t)$ of the solid substance as

$$\alpha(t) = \frac{m_0 - m(t)}{m_0 - m_\infty}, \tag{2}$$

where m_0 is the initial mass of the solid and m_∞ is the mass of the solid residue after complete decomposition (the char).

The dependence of the reaction rate on temperature is commonly described by the Arrhenius equation [32]

$$k(T(t)) = \mathscr{A} \exp\left\{ \frac{-\mathscr{E}}{\mathscr{R} T(t)} \right\}, \tag{3}$$

where $k(T(t))$ is the constant rate (s^{-1}), $\mathscr{R}$ is the universal gas constant (J K^{-1} mol^{-1}), $\mathscr{A}$ is the pre-exponential factor (s^{-1}) and $\mathscr{E}$ is the activation energy (J mol^{-1}). In gas reactions, $\mathscr{A}$ is interpreted as the frequency of molecular collision and $\mathscr{E}$ is the energy that must be provided for the reaction to occur. The use of the Arrhenius equation for solid-state reactions and the actual meaning of these kinetic parameters, contrary to gas reactions, is still subject to debate [32]. A possible interpretation for $\mathscr{A}$ is the frequency factor or specific vibration of the reactant and for $\mathscr{E}$ the energy barrier that must be surmounted during the bond redistribution occurring during the phase change [26,47].

Temperature is not the only factor influencing the rate of the pyrolysis process: it may depend on the fractional decomposition factor α and the pressure of volatile

products (in case of gas-solid reaction) p_j. This leads to the following more general formulation for the evolution of the solid

$$\frac{d\alpha}{dt}(t) = k(T(t))\, f(\alpha(t))\, g(p_j(t))\,. \tag{4}$$

The dependence on the partial pressure is ignored in most kinetic studies [31]. The dependence on the fractional decomposition (the reaction model) can be generically formulated as $f(\alpha) = \alpha^l(1-\alpha)^n\,[-\ln(1-\alpha)]^r$ as proposed by Šesták-Berggren [27, 28]. Typical aerospace applications assume a reaction-order model, i.e. $l = 0, r = 0$, for the dependence on the advancement reaction: $f(\alpha) = (1-\alpha)^n$, with n the order of reaction. There are two reasons here for considering this particular form for the reaction model. The first one is because the integration of this single-parameter reaction-order model results in a closed-form solution. For instance, the reaction model $f(\alpha) = \alpha^l(1-\alpha)^n$, as in Zhang et al. [25], would result in a solution that involves the incomplete beta function. The second one is the long legacy of previous pyrolysis modeling of TPMs that assumed this kinetic model and which provided satisfactory results.

This finally leads to the following ordinary differential equation (ODE) for pyrolysis with the one-parameter Šesták-Berggren kinetic model

$$\frac{d\alpha}{dt}(t) = \mathscr{A} \exp\left\{\frac{-\mathscr{E}}{\mathscr{R}T(t)}\right\}(1-\alpha(t))^n\,. \tag{5}$$

This ODE represents the advancement of the reaction for a point mass sample, which is a good approximation for many thermoanalytical experiments [11]. It can be extended to more complex cases by considering an energy equation that include the thermal conductivity within the material or the heat capacity of the material, in which case the temperature is a function of space and time and the ordinary differential equation is replaced by a partial differential equation [48, 13, 15].

Sometimes, the pre-exponential factor is expressed as $\mathscr{A} = \mathscr{A}_0 T^m$, where A_0 denotes a temperature-independent factor, in order to emphasize a potential dependence on temperature [38]. Previous work on parameter identification for thermal protection materials showed that the parameter m tends to zero [11], so in the following we will set $m = 0$ and omit T^m for simplicity. Therefore, the kinetic triplet ($\mathscr{A}$, $\mathscr{E}$ and n) is assumed to be independent of temperature and we assume in the following that $\mathscr{A} > 0$, $\mathscr{E} > 0$ and $n \geq 1$.

2.1.2 Multi-component kinetic equations

In most cases, solid state reactions are often too complex to be described using a single reaction [49, 29]. The global reaction mechanism is encapsulated within phenomenologically coherent steps describing the elementary unknown processes. It is therefore convenient to define multiple advancement of reaction factors $0 \leq \alpha_i \leq 1$, where $1 \leq i \leq N_\mathrm{p}$ idexes independent pyrolysis reactions occurring in parallel and N_p is the number of pyrolysis decomposition processes present in the solid resin (or the number of reactants, or the number of steps). Each step represents a distinct reactant

(or sub-phase) in the solid [13]. The corresponding reaction scheme is represented schematically in Eq. 6:

$$\mathrm{R}^{(s)} \begin{cases} \nearrow & w_1\mathrm{R}_1^{(s)} \xrightarrow{k_1} \mathrm{C}^{(s)} + \gamma_{11}S_1^{(g)} + \gamma_{12}S_2^{(g)} + \cdots + \gamma_{1j}S_j^{(g)} \\ \longrightarrow & w_2\mathrm{R}_2^{(s)} \xrightarrow{k_2} \mathrm{C}^{(s)} + \gamma_{21}S_1^{(g)} + \gamma_{22}S_2^{(g)} + \cdots + \gamma_{2j}S_j^{(g)} \\ & \vdots \\ \searrow & w_i\mathrm{R}_i^{(s)} \xrightarrow{k_i} \mathrm{C}^{(s)} + \gamma_{i1}S_1^{(g)} + \gamma_{i2}S_2^{(g)} + \cdots + \gamma_{ij}S_j^{(g)} \end{cases} \tag{6}$$

where w_i is the relative weight, or mass fraction of compound R_i from the virgin reactant R and $\sum_{i=1}^{N_\mathrm{p}} w_i = 1$. The evolution of the N_p advancement of reaction factors given the reaction scheme Eq. 6 is therefore

$$\frac{d\alpha_i}{dt}(t) = \mathscr{A}_i \exp\left\{\frac{-\mathscr{E}_i}{\mathscr{R}T(t)}\right\}(1-\alpha_i(t))^{n_i}, \quad 1 \leq i \leq N_\mathrm{p}. \tag{7}$$

This expression is widely used in the aerospace community to model thermal protection materials pyrolysis [50–58, 15, 13, 16]. We refer to this process as multi-step, multi-component, or parallel pyrolysis reactions. The advancement of reaction factors are defined for the compounds R_i of mass $m_i(t)$ as

$$\alpha_i(t) = \frac{m_{0,i} - m_i(t)}{m_{0,i} - m_{\infty,i}}, \quad 1 \leq i \leq N_\mathrm{p} \tag{8}$$

and we have $\alpha(t) = \sum_{i=1}^{N_\mathrm{p}} w_i\alpha_i(t)$. The total mass of the sample can then be obtained by inserting the latter in Eq. 2. The parameters w_i are unknown, and m_∞ can also be an unknown if the reaction process did not reach completion at the end of the temperature program and therefore cannot be measured experimentally, as it is the case in Bessire et al. [10]. Moreover, it was observed that the constraint $\sum_{i=1}^{N_\mathrm{p}} w_i = 1$ was difficult to satisfy when performing the calibration of kinetic parameters [16]. In order to reduce by one the number of unknown parameters and avoid the need to satisfy $\sum_{i=1}^{N_\mathrm{p}} w_i = 1$, we can assume that the total mass at the end of the process m_∞ expresses as a function of the initial mass as $m_\infty = F_\infty m_0$. Thus, we can write $F_i = w_i(1-F_\infty)$ such that the total mass is finally given by

$$m(t) = m_0 - \sum_{i=1}^{N_\mathrm{p}} \alpha_i(t)F_i m_0. \tag{9}$$

Note that now $\sum_{i=1}^{N_\mathrm{p}} F_i \leq 1$ and the mass after completion of the reaction can be retrieved by computing $m_\infty = m_0(1 - \sum_{i=1}^{N_\mathrm{p}} F_i)$.

2.1.3 Pyrolysis gas production

The advancement of reaction factors α_i cannot be observed directly from experiments; thus, for calibrating model parameters, we need to provide a mathematical expression for the model output that can be linked to the experimental observations. TGA allows to measure the mass loss that is linked to the α_i through Eq. 9 and pyrolysis products can be observed using a mass spectrometer, for instance, as in Bessire et al. [10]. The pyrolysis species production allows to observe more accurately the independent reaction steps. Although production rate can also be obtained by differentiating the TGA data, the differentiation introduces however additional numerical noise in the experimental data. We will therefore consider the pyrolysis species production as the observable as it is also used in Torres-Herrador et al. [11].

During pyrolysis, part of the solid material is converted into gas and pyrolysis gas production can be obtained from mass conservation. It is assumed that char and gaseous species are the only products from pyrolysis. Because the char is non-volatile, mass variation of the sample is necessarily linked to the pyrolysis gas production and any sample mass decrease implies pyrolysis gas production. Thus, the pyrolysis gas production rate is given by

$$\pi(t) = -\frac{dm}{dt}(t) = \sum_{i=1}^{N_p} F_i \frac{d\alpha_i}{dt}(t) m_0 = \sum_{i=1}^{N_p} \pi_i(t), \tag{10}$$

where $\pi_i(t) = F_i \frac{d\alpha_i}{dt}(t) m_0$ is the mass production rate coming from the decomposition of the reactant i. The last equality on the right-hand side of Eq. 10 is the total production rate defined as the sum of the contributions of all the reactants that are decomposing. The production of species j, required when we need to track species in flow simulations, is obtained from $\nu_{ij}(t) = \gamma_{ij}\pi_i(t)$ where γ_{ij} is the mass fraction of species j produced from reaction i. Finally, the total production of species j is obtained as

$$\nu_j(t) = \sum_{i=1}^{N_p} \nu_{ij}(t) = \sum_{i=1}^{N_p} \gamma_{ij}\pi_i(t). \tag{11}$$

2.2 Analytical solution of the multi-component model with the one-parameter Šesták-Berggren equation

An analytical solution does not necessarily exist when the temperature program is an arbitrary function of time. However, most experimental studies such as in TGA are carried out by using either a linearly increasing temperature $T = \beta(t - t_0) + T_0$ with β the heating rate in $\mathrm{K\,min^{-1}}$ ([10,11]), t_0 the initial time and T_0 the initial temperature, or constant temperature $T = \text{const}$ (isothermal conditions) ([8,9,59]). The case of a linearly increasing temperature is widely used in thermal protection materials decomposition studies [50,60,52,10,11,61]. For constant temperature, some experimental set-ups use a piecewise constant temperature program [8,9], where the

isothermal condition is maintained only during a given time interval. In these settings, the temperature $T(t)$ is maintained at a constant value $T^{(k)}$ during a time interval $A^{(k)} = \left[t_0^{(k)}, t_\mathrm{f}^{(k)}\right]$ in order to collect and analyze the species products before increasing the temperature to its next value $T^{(k+1)}$. The temperature is thus assumed to be the piecewise constant function $T(t) = T^{(k)}$ for all $t \in A^{(k)}$ with $1 \leq k \leq n_\mathrm{step}$ and n_step the number of temperature increase.

Therefore, we wish to find the analytical solution to the initial-value problem (IVP)

$$\begin{cases} \dfrac{d\alpha_i}{dt}(t) = \mathscr{A}_i \exp\left\{\dfrac{\mathscr{E}_i}{\mathscr{R}T(t)}\right\}(1-\alpha_i(t))^{n_i}, \text{ for} t > t_0, \\ \alpha_i(t_0) \;\; = \alpha_{i,0}, \qquad\qquad\qquad\qquad\qquad\qquad i = 1,\ldots,\mathrm{N_p} \end{cases} \tag{12}$$

with either

$$T(t) = \text{const} \quad \text{(isothermal)} \tag{13}$$

or

$$T(t) = \beta(t-t_0) + T_0 \quad \text{(linearly increasing temperature)}. \tag{14}$$

The system of equations in (12) is a system of independent first-order non-linear ODEs with constant coefficients in the case of (13) and with non-constant coefficients in the case of (14). We start by performing a simple change of variables as follows. Substituting $u_i(t) = 1 - \alpha_i(t)$ leads to

$$\frac{du_i(t)}{dt} = -u_i^n(t)\mathscr{A}_i \exp\left\{\frac{-\mathscr{E}_i}{\mathscr{R}T(t)}\right\}. \tag{15}$$

Dividing both handsides by $u_i^{-n}(t)$, assumed nonzero, and integrating both sides of the equation with respect to time, we have

$$-\int_{t_0}^{t} u_i^{-n}(\tilde{t})\frac{du_i(\tilde{t})}{d\tilde{t}}d\tilde{t} = \int_{t_0}^{t} \mathscr{A}_i \exp\left\{\frac{-\mathscr{E}_i}{\mathscr{R}T(\tilde{t})}\right\}d\tilde{t}, \tag{16}$$

where the right-hand side is the integral of the Arrhenius equation and is named the temperature integral

$$I_i(t) = \int_{t_0}^{t} \mathscr{A}_i \exp\left\{\frac{-\mathscr{E}_i}{\mathscr{R}T(\tilde{t})}\right\}d\tilde{t}. \tag{17}$$

The case where $n_i = 1$ is left for the end of the section. Assuming that $n_i \neq 1$, the left-hand side can be integrated by substitution leading to

$$-\int_{u_i(t_0)}^{u_i(t)} \tilde{u}^{-n}d\tilde{u} = -\frac{1}{1-n_i}\left(u_i^{1-n_i}(t) - u_i^{1-n_i}(t_0)\right). \tag{18}$$

Inserting this expression in Eq. 16 and finally expressing the result with the advancement of reaction factor, we obtain

$$u_i(t) = \left(u_i^{1-n_i}(t_0) - I_i(t)(1-n_i) \right)^{1/(1-n_i)}, \tag{19}$$

$$\alpha_i(t) = 1 - \left((1-\alpha_i(t_0))^{1-n_i} - I_i(t)(1-n_i) \right)^{1/(1-n_i)}. \tag{20}$$

In this last equation, we still need to provide an expression for the temperature integral $I_i(t)$, that depends on time through the temperature program.

2.2.1 Case 1: piecewise isothermal

In isothermal pyrolysis experiments, we assume the temperature to be constant on a given time interval $A = [t_0, t_\mathrm{f}]$. Thus $I_i(t)$ is easily integrated on the time interval, leading to

$$I_i(t) = \mathscr{A}_i \exp\left\{ \frac{-\mathscr{E}_i}{\mathscr{R}T} \right\} (t - t_0). \tag{21}$$

For completeness, we consider the more general case of a piecewise constant temperature as a function of time; this procedure is applied, for instance, in Wong et al. [8, 9]. The overall experiment is seen as the succession of n_step smaller experiments with advancement of reaction factors $\alpha_i^{(k)}(t)$ where the initial condition $\alpha_i^{(k)}(t_0)$ depends on the state of the material at the end of the previous time interval. The temperature $T^{(k)}$ is maintained constant during the time interval $A^{(k)} = \left[t_0^{(k)}, t_\mathrm{f}^{(k)} \right]$ and is equal to $T^{(k+1)}$ in the next interval. The transient part of temperature increase between each time interval is neglected because of its short duration compared to the whole process. The solution for the advancement of reaction factor as a function of time in the k interval is therefore

$$\alpha_i^{(k)}(t) = 1 - \left(\left(1 - \alpha_i^{(k)}(t_0^{(k)}) \right)^{1-n_i} - (1-n_i)\mathscr{A}_i \exp\left\{ \frac{-\mathscr{E}_i}{\mathscr{R}T^{(k)}} \right\} (t - t_0^{(0)}) \right)^{1/(1-n_i)}, \tag{22}$$

and the solution is $\alpha_i(t) = \alpha_i^{(k)}(t)$ for all $A^{(k)}$. Usually $\alpha_i^{(0)}(t_0^{(0)}) = 0$ in the first time interval, then the value for $\alpha_i^{(k)}(t_0^{(k)})$ in a given time interval is equal to $\alpha_i^{(k-1)}(t_\mathrm{f}^{(k-1)})$ from the previous time interval. This expression simplifies further if we set $t_0^{(k)} = 0 \; \forall \; k$. If $n_\mathrm{step} = 1$, then the solution is for a single isothermal condition.

2.2.2 Case 2: linearly increasing temperature

In this case, the temperature increases linearly with time until the end of the experiment, thus $T = \beta(t - t_0) + T_0$ and

$$I_i(t) = \int_{t_0}^{t} \mathscr{A}_i \exp\left\{ \frac{-\mathscr{E}_i}{\mathscr{R}(\beta(\tilde{t} - t_0) + T_0)} \right\} d\tilde{t}. \tag{23}$$

For the computation of $I_i(t)$, we apply the following change of variables: $v_i = -\mathscr{E}_i/(\mathscr{R}(\beta(t-t_0)+T_0))$ thus $dt = \mathscr{E}_i/(\mathscr{R}\beta v_i^2)dv_i$. The integral becomes

$$\begin{aligned} I_i(t) &= \int_{v_{i,0}}^{v_i} \frac{\mathscr{A}_i}{\beta}\frac{\mathscr{E}_i}{\mathscr{R}\tilde{v}^2}\exp\{\tilde{v}\}\,d\tilde{v} \\ &= \frac{\mathscr{A}_i}{\beta}\frac{\mathscr{E}_i}{\mathscr{R}}\int_{v_{i,0}}^{v_i}\frac{\exp\{\tilde{v}\}}{\tilde{v}^2}d\tilde{v} \\ &= \frac{\mathscr{A}_i}{\beta}\frac{\mathscr{E}_i}{\mathscr{R}}\left(\left[-\frac{\exp\{\tilde{v}\}}{\tilde{v}}\right]_{v_{i,0}}^{v_i} + \int_{v_{i,0}}^{v_i}\frac{\exp\{\tilde{v}\}}{\tilde{v}}d\tilde{v}\right), \end{aligned} \tag{24}$$

where the last line results from the integration by parts. The second summand on the right-hand side is the exponential-integral function [62]

$$\mathrm{Ei}(v) = \int_{-\infty}^{v}\frac{\exp(\tilde{v})}{\tilde{v}}d\tilde{v} \quad (v>0). \tag{25}$$

Thus, inserting the exponential-integral function into Eq. 24 leads to

$$\begin{aligned} I_i(t) &= \frac{\mathscr{A}_i}{\beta}\frac{\mathscr{E}_i}{\mathscr{R}}\left[-\frac{\exp\{\tilde{v}\}}{\tilde{v}} + \mathrm{Ei}(\tilde{v})\right]_{v_{i,0}}^{v_i(t)} \\ &= \frac{\mathscr{A}_i}{\beta}\frac{\mathscr{E}_i}{\mathscr{R}}\left(-\frac{\exp\{v_i(t)\}}{v_i(t)} + \frac{\exp\{v_{i,0}\}}{v_{i,0}} + \mathrm{Ei}(v_i(t)) - \mathrm{Ei}(v_{i,0})\right) \\ &= \frac{\mathscr{A}_i}{\beta}\frac{\mathscr{E}_i}{\mathscr{R}}\left(\frac{\mathscr{R}T(t)}{\mathscr{E}_i}\exp\left\{\frac{-\mathscr{E}_i}{\mathscr{R}T(t)}\right\} - \frac{\mathscr{R}T_0}{\mathscr{E}_i}\exp\left\{\frac{-\mathscr{E}_i}{\mathscr{R}T_0}\right\}\dots\right. \\ &\left.+\mathrm{Ei}\left\{\frac{-\mathscr{E}_i}{\mathscr{R}T(t)}\right\} - \mathrm{Ei}\left\{\frac{-\mathscr{E}_i}{\mathscr{R}T_0}\right\}\right). \end{aligned} \tag{26}$$

This can be inserted into Eq. 20 to obtain the final expression of the advancement coefficient of each reactant i as a function of time.

Usually, the advancements of reaction are plotted against temperature instead of time for convenience. Gathering the terms that depend on temperature, we can write

$$\alpha_i = 1 - \left\{(1-n_i)\left[-\frac{\mathscr{A}_i}{\beta}T\exp\left\{\frac{-\mathscr{E}_i}{\mathscr{R}T}\right\} - \frac{\mathscr{A}_i}{\beta}\frac{\mathscr{E}_i}{\mathscr{R}}\mathrm{Ei}\left\{\frac{-\mathscr{E}_i}{\mathscr{R}T}\right\} + C_i\right]\right\}^{\frac{1}{1-n_i}}, \tag{27}$$

$$C_i = \frac{(1-\alpha_i(T_0))^{1-n_i}}{1-n_i} + \frac{\mathscr{A}_i}{\beta}T_0\exp\left\{\frac{-\mathscr{E}_i}{\mathscr{R}T_0}\right\} + \mathrm{Ei}\left\{\frac{-\mathscr{E}_i}{\mathscr{R}T_0}\right\}\frac{\mathscr{A}_i\mathscr{E}_i}{\beta\mathscr{R}}. \tag{28}$$

For the test case in Sect. 4 we will consider the gas production from Eq. 11. Thus, the gas production rate for species j is given by (with $F_{ij} = \gamma_{ij}F_i$)

$$\nu_j = \sum_{i=1}^{N_p} m_0 F_{ij}\beta\frac{d\alpha_i}{dT}, \tag{29}$$

and inserting the analytical solution gives

$$\nu_j = \sum_{i=1}^{N_p} m_0 F_{ij} \left(\left\{ (1-n_i) \left[-\frac{\mathscr{A}_i}{\beta} T \exp\left\{ \frac{-\mathscr{E}_i}{\mathscr{R}T} \right\} \dots \right.\right.\right.$$
$$-\frac{\mathscr{A}_i}{\beta}\frac{\mathscr{E}_i}{\mathscr{R}} \mathrm{Ei}\left\{ \frac{-\mathscr{E}_i}{\mathscr{R}T_0} \right\} + \frac{(1-\alpha_{i,0})^{1-n_i}}{1-n_i} + \frac{\mathscr{A}_i}{\beta} T_0 \exp\left\{ \frac{-\mathscr{E}_i}{\mathscr{R}T_0} \right\} \dots$$
$$\left.\left.\left. +\mathrm{Ei}\left\{ \frac{-\mathscr{E}_i}{\mathscr{R}T_0} \right\} \frac{\mathscr{E}_i \mathscr{A}_i}{\beta} \right] \right\}^{\frac{1}{1-n_i}} \right)^{n_i} \mathscr{A}_i \exp\left\{ \frac{-\mathscr{E}_i}{\mathscr{R}T} \right\}. \tag{30}$$

Finally, computation of derivatives with respect to parameters are provided in Appendix A.

2.2.3 Particular case: linear Šesták-Berggren model

The case of $n_i = 1$ in Eq. 7 results in a linear system of uncoupled ODEs that is now addressed in this section for the two heating conditions.

We substitute $n_i = 1$ in Eq. 16 and the left-hand side leads to

$$\ln(u_{i,0}) - \ln(u_i(t)) = I_i(t). \tag{31}$$

For the (piecewise) isothermal case, with $I_i(t)$ from Eq. 21, this leads to

$$\alpha_i^{(k)}(t) = 1 - (1-\alpha_{i,0}^{(k)}) \exp\left(-\mathscr{A}_i \exp\left\{ \frac{-\mathscr{E}_i}{\mathscr{R}T} \right\} (t - t_0^{(k)}) \right). \tag{32}$$

For the linearly increasing temperature, we substitute $I_i(t)$ from Eq. 26, thus leading to

$$\alpha_i = 1 - C_i \exp\left\{ -\frac{\mathscr{A}_i}{\beta} T \exp\left\{ \frac{-\mathscr{E}_i}{\mathscr{R}T} \right\} - \frac{\mathscr{A}_i}{\beta}\frac{\mathscr{E}_i}{\mathscr{R}} \mathrm{Ei}\left\{ \frac{-\mathscr{E}_i}{\mathscr{R}T} \right\} \right\}, \tag{33}$$

$$C_i = (1-\alpha_{i,0}) \exp\left\{ \frac{\mathscr{A}_i}{\beta} T_0 \exp\left\{ \frac{-\mathscr{E}_i}{\mathscr{R}T_0} \right\} + \frac{\mathscr{A}_i}{\beta}\frac{\mathscr{E}_i}{\mathscr{R}} \mathrm{Ei}\left\{ \frac{-\mathscr{E}_i}{\mathscr{R}T_0} \right\} \right\}. \tag{34}$$

2.2.4 Matrix formalism

The case of $n_i = 1$ can be written using a matrix formalism thanks to the linearity of the equations. This partiular case of $n_i = 1$ was already considered in the more general framework of competitive reaction mechanisms in [63] where the system of ODEs is no longer uncoupled.

Using the change of variables $u_i(t) = 1 - \alpha_i(t)$, the general reaction mechanisms Eq. 6 with Eq. 7 governing the evolution of the advancement and $n_i = 1$ can be written as

$$\frac{du}{dt} = A(t)u, \tag{35}$$

where $A(t)$ is a square matrix whose coefficients are a linear combination of the reaction rates k_i and depend on time. In the case of a multi-component pyrolysis model such as the one presented here, the matrix A is diagonal with $A_{ii} = -k_i$.

3 Materials and methods

The materials considered in this study are composites made up of short carbon fibers infused with a phenolic resin that are used in the thermal protection system of spacecraft. In particular, we consider the phenolic-impregnated carbon ablator (PICA) that has been successfully used in previous space mission for his excellent thermal protection performances.

The heating rates encountered during an actual re-entry application largely vary within the heatshield. In addition, they may be significantly higher than current ground testing techniques. In the experiments of Bessire et al. [10], the pyrolysis of PICA material was performed at significantly different heating rate values, namely 186, 366, 762 and 1500 $\mathrm{K\,min^{-1}}$. In [10], the PICA sample is heated from 375 to 1400 K in a vacuum chamber by means of an electrical current that passes through the sample. In-situ measurements of PICA pyrolysis product yields are performed using mass spectrometry, which provided the product yields of 14 gaseous species as a function of the material temperature.

Torres-Herrador et al. [16] performed a model calibration using a multi-component approach from the results from the experiments of Bessire et al. [10] at the heating rate $\beta = 360\ \mathrm{K\,min^{-1}}$. Six components ($N_\mathrm{p} = 6$) were identified in the pyrolysis model by visual inspection of the maximum species production peaks in order to simulate the production of the 14 observed gas products. A model fitting procedure was then performed using a multi-objective genetic algorithm (MOGA) and the pyrolysis model was implemented in the software PATO [57] and integrated in time using a first-order implicit scheme. The 24 kinetic parameter and mass fraction values resulting from the fitting procedure of the six-reaction model are summarized in Table 1. We note that the mass fractions F_i had to be updated compared to [16] because the model presented here considers the pyrolysis of a pure resin, while Eq. 9 is not considering the mass of non-pyrolyzing phases (carbon fibers). Therefore, for the normalization of the variable with the total mass of the composite, we have to multiple F_i by a factor equal to $m_0/(m_0 + m_\mathrm{fibers})$ which is around 0.43 (PICA contains a 43% of resin in mass). The sample mass and the mass production rates π_i from the decomposition of each component for the calibrated pyrolysis model are shown in Fig. 1. The six-reaction pyrolysis model with the calibrated species mass fractions is as follows:

$$F_1\mathrm{R}_1^{(s)} \xrightarrow{k_1} 0.62\mathrm{H_2O} + 0.38\mathrm{CO}$$

$$F_2\mathrm{R}_2^{(s)} \xrightarrow{k_2} 0.69\mathrm{CO_2} + 0.21\mathrm{C_3H_8O_{,1}} + 0.09\mathrm{C_3H_8O_{,2}}$$

$$F_3\mathrm{R}_3^{(s)} \xrightarrow{k_3} 0.42\mathrm{H_2O} + 0.06\mathrm{CO_2} + 0.15\mathrm{C_6H_6O} + 0.34\mathrm{C_7H_8O} + 0.03\mathrm{C_8H_{10}}$$

$$F_4\mathrm{R}_4^{(s)} \xrightarrow{k_4} 0.67\mathrm{CO} + 0.27\mathrm{CH_4} + 0.03\mathrm{C_6H_6} + 0.04\mathrm{C_7H_8}$$

$$F_5\mathrm{R}_5^{(s)} \xrightarrow{k_5} \mathrm{H_2}$$

$$F_6\mathrm{R}_6^{(s)} \xrightarrow{k_4} 0.19\mathrm{H_2} + 0.81\mathrm{CO}$$

The pyrolysis of phenolic resins, like in PICA, is typically divided into four overlapping stages [64,65,60,9,10], which can be related to the six components of the

Table 1 Parameter values for the six-reaction pyrolysis model from [16], with the F parameters re-scaled in order to consider the pyrolysis of a pure resin.

R	F	$\log(\mathscr{A})$ (s^{-1})	$\mathscr{E}$ (kJ mol^{-1})	n
1	0.0039	6.96	61.3	9.96
2	0.0258	6.59	77.6	5.65
3	0.0873	6.71	95.1	4.23
4	0.0804	6.67	103.0	4.38
5	0.0112	6.58	113.9	6.68
6	0.0254	6.35	175.2	8.85

pyrolysis reaction model from above and the resulting mass production rates π_i from Fig. 1b. In the first stage, water observed at low temperatures around 400 K (π_1 in Fig. 1b) is usually attributed to humidity (outgassing) [10]. In stage 2, two competing major processes were identified at temperatures in the range 575 – 785 K: cross-linking reactions releasing H_2O while forming ether and carbon—carbon bonds, and scission of methylene brides releasing phenol and its methylated derivatives (π_3). Stage 3 corresponds to the generation of CO and CH_4 due to reactions that, in the current literature, are not yet clearly understood (π_4): Ouchi and Honda [64] identified, for instance, a two-step mechanism while Trick and Saliba [60] identified a one-step mechanism. Finally, stage 4 occurs at high temperatures ($\geq$ 1000 K), where H_2 is the major product due to the formation of stable char (π_5 and π_6). The CO observed at high temperatures does not have a clear origin, but it was included in π_6. Remaining gases that do not have a clear reaction were included in a reaction corresponding to their production peaks, such as CO at low temperature (π_1) or xylene (π_3), or to a new reaction (π_2), such as for isopropanol.

The two mechanisms in stage 2 are in competition with each other, meaning that the products resulting from these processes are generated in varying proportions depending on the heating rate. Hence, a pyrolysis model that accounts for competitive mechanisms should ideally be considered for the decomposition of PICA when the heating rate value is varied significantly [66]. However, competitive mechanisms are not considered in the multi-component model described in Sect. 2.1.2. Therefore, we will illustrate the analytical solution for the pyrolysis of PICA at a single heating rate.

4 Results

In this last section, we illustrate the efficiency of the implemented analytical solution by comparing it with a numerical solution of the non-linear system of ODEs. We consider the pyrolysis scheme described in Torres-Herrador et al. [16] based on the experiments of Bessire et al. [10] that was described in the previous section. We verify the accuracy of the analytical solution and we show the computational gain achieved by using it in a case involving a linearly increasing temperature. We finally perform a sensitivity analysis to illustrate the use of the derivatives with respect to parameters.

4.1 Comparison of the analytical solution with a numerical solution

The solutions (both analytical and numerical) to the pyrolysis equations and their derivatives are implemented in an in-house Python code. The exponential-integral function is computed using the `special.expi()` function from the `scipy` library. Its implementation is based on a fortran implementation of the series expansion of the exponential-integral Ei(x) (with $x > 0$) [62]. For the numerical solution, the integration of the system of ODEs is performed using the `integrate.solve_ivp()` function from the scipy library. In particular, it features an implicit multi-step Runge-Kutta method of the Radau IIA family of order 5 [67]. Indeed, chemical reactions involving the Arrhenius equation can be stiff, i.e. there can be a rapid variation of the solution due to a fast degradation of a reactant compared to an other one, and for generality we decided to use a numerical solver capable of dealing with these different reaction scales [68]. The varying time step is determined by the solver that keeps a relative tolerance, which controls the number of correct digits, that we set to 10^{-8}.

The numerical solution, the analytical solution and their derivatives are computed at 101 points in the temperature range with the parameter values from Table 1. The comparison of the analytical solution with the numerical solution is shown in Fig. 1. The solution is shown for the mass loss in Fig. 1a and the total gas production in Fig. 1b. The quantities on the y-axis are normalized by the total mass of the composite. Mass loss of the material is computed from Eqs. 28 and 27 and the production of pyrolysis gas is computed from Eq. 30 and we can see from Fig. 1 that the two solutions match. The relative errors of the analytical solution compared to the numerical solution are computed as

$$\mathrm{err}(T) = \left| \frac{y_{\mathrm{analytical}}(T) - y_{\mathrm{numerical}}(T)}{y_{\mathrm{numerical}}(T)} \right|. \tag{36}$$

For the mass of the material, we have $\mathrm{err}(T) \leq 2.5 \times 10^{-8}$ which is of the order of magnitude of the relative tolerance set to the numerical solver and show that the analytical solution is computed with high accuracy. For the total gas production, we have $\mathrm{err}(T) \leq 6.2 \times 10^{-6}$, which is higher than for the mass because the reaction process rate needs to be recomputed from Eq. 12.

In Fig. 1b, we also show the production rate π_i coming from the decomposition of each reaction i with $\pi = \sum_{i=1}^{N_\mathrm{p}} \pi_i$ to identify the different contributions of all reactions to the global production rate.

Derivatives are computed numerically using a first-order finite-difference formula by perturbing one by one the parameters about their nominal value. Each perturbed solution is computed using the analytical expressions Eqs. 37–46 (sensitivities of π and ν are the same here because we considered only one species). Results for the 24 derivatives are shown in Fig. 2. Once again, the two solutions match over the whole temperature range.

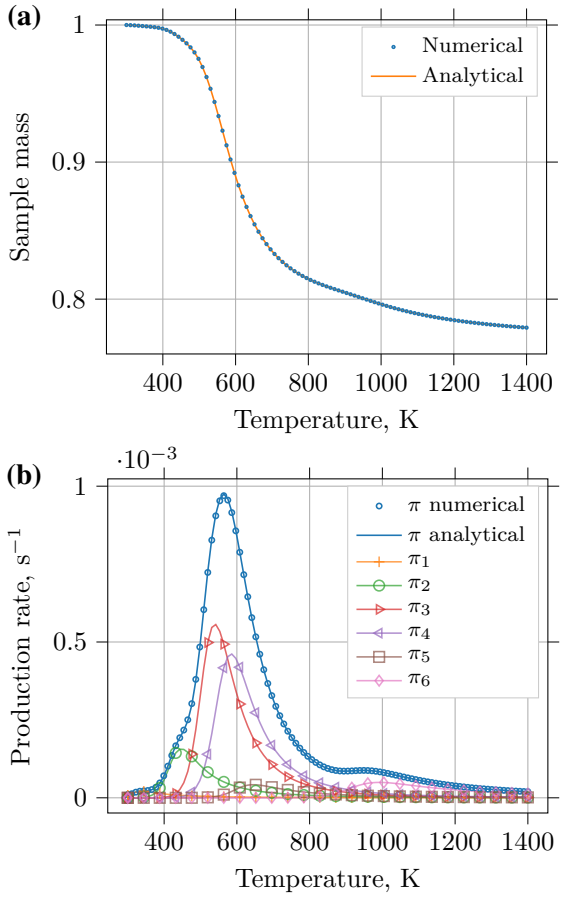

Fig. 1 Comparison of the solution obtained from the analytical solution and the numerical integration for **(a)** the sample mass and **(b)** the total production rate.

4.2 Computational gain for parameter inference

In order to illustrate the computational gain of this solution, we compared the execution time to compute 600 times the solution, which corresponds to the initial sample size for the MOGA algorithm in [16]. Thus, the following analysis only characterizes the computational time for the initialization of the MOGA algorithm, but the total number of model evaluations is higher. Parameter values are kept constant, but we should keep in mind that varying them with the iterations could influence the computational time of the numerical solution. The computations are performed on a single CPU Intel Core i7-6820HQ using a single thread. The time to compute the 600 solutions numerically took 42.46 s while the analytical evaluations took 0.29 s, which is almost 150 times faster. Although they are not used in the MOGA algorithm, we can estimate the time that the derivatives would take to be computed. For the numeri-

cal computation of the derivatives, we need one additional model evaluation for each perturbed parameter for the finite difference evaluation that would be approximately 24×42.46 s (≈ 17 min), while the 600 analytical evaluations of the derivatives is taking approximately 3.35 s, which is approximately 300 times faster.

It is also important to note that the computational time increases proportionally with the number of equations in the model N_p (and so the complexity of the pyrolysis model). This increase in the computational time is more impacted by the number of equations with the numerical solution because of the adaptive time-step procedure and the time to compute the Jacobian matrix (derivative of the right-hand side of Eq. 12 with respect to t) needed for the implicit Radau IIA method, which was evaluated by the solver using finite differences.

4.3 Local sensitivity analysis

Finally, we perform a local sensitivity analysis from the graph of the sensitivities in Fig. 2. We can first observe the compensation effect between $\mathscr{A}$ and $\mathscr{E}$ (for both i) from Fig. 2a and 2b: we see from the graphs that they have opposite effects on the solution (because $\mathscr{E}$ appears with a negative sign in the exponential). This means that an increase of $\mathscr{A}$ can be compensated by a decrease of $\mathscr{E}$ while keeping the value of the solution π almost constant. This will result in a wide range of possible values for $\mathscr{A}$ and $\mathscr{E}$ when calibrating their values from experiments and explains the hurdle of calibrating them at the same time. We also see that the sensitivity of π with respect to $\mathscr{E}$ is roughly three orders of magnitude higher than with $\mathscr{A}$ and due to the fact that $\mathscr{E}$ appeared in the exponential term.

Regarding the order of magnitudes of all the parameters, we see that the F_i parameters have the highest impact on the solution π, followed by n_i and finally $\mathscr{E}_i$ and $\mathscr{A}_i$. F_i has the biggest impact on the production as it influences directly the production of char and is positive everywhere. Increasing F_i will always result in an increase of the gas produced from the pyrolysis reaction and less char left at the end of the process. The shape of the curves for $\mathscr{E}_i$ and n_i is almost the same, with a little shift in temperature and with three orders of magnitude difference. Finally, we note that reaction 1 has a high influence on the production rate despite its lowest contribution to the total mass ($F_1 = 0.00039$). Comparatively, reaction 5 and 6 have higher mass fractions, but $\partial\pi/F_i$ (Fig. 2d) is lower than for reaction 1. This is due to the fact that changes in the mass fraction of the first reaction will impact the subsequent productions rates.

This short analysis is valid locally about the nominal parameter values and provides a good overview of the relative influence of the parameters. We should also keep in mind that the analysis might be slightly different with a different combination of the nominal parameters. Finally, a global sensitivity analysis should be performed to give a more global overview of the impact of the parameters on the solution.

5 Conclusion

We presented an analytical solution for multi-component pyrolysis models with an arbitrary number of pyrolysis reactions and featuring the one-parameter Šesták-Berggren

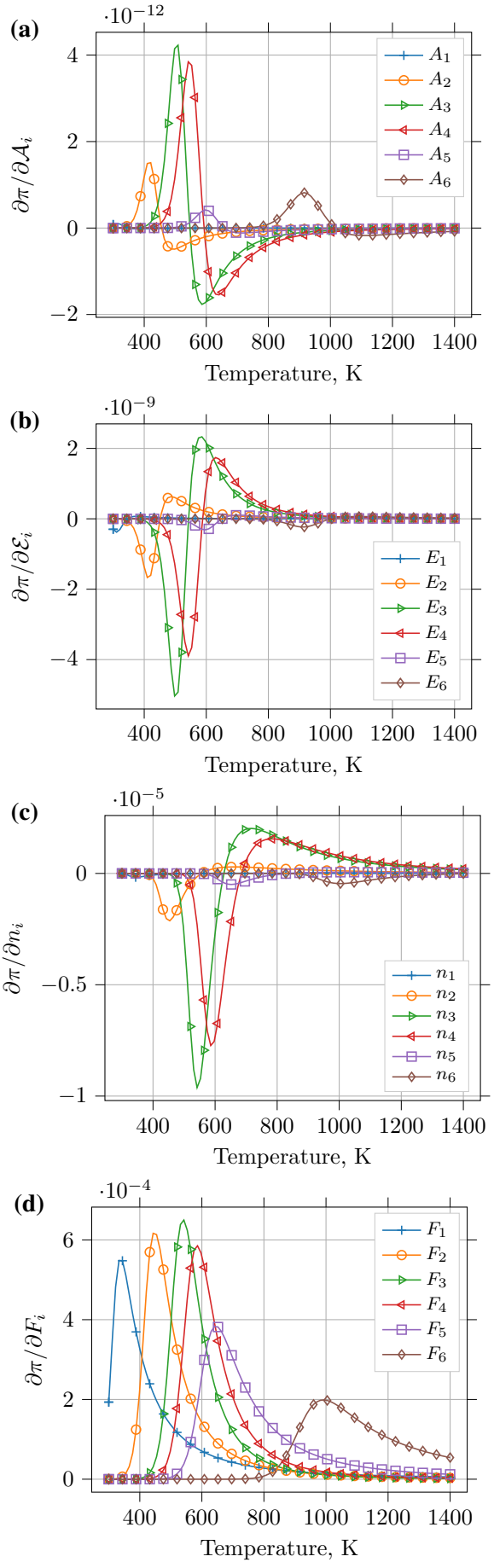

Fig. 2 Comparison of the sensitivities computed analytically and using finite differences (numerical) with respect to the 24 parameters: **(a)** pre-exponential factors $\mathscr{A}_i$, **(b)** activation energies $\mathscr{E}_i$, **(c)** reaction orders n_i and **(d)** mass fractions F_i. The continuous and discontinuous lines are for the analytical solutions and the markers for the numerical solutions. For the clarity of the images, we displayed only 25 markers instead of the 101 points where the solution were computed.

kinetic model. The solution of the temperature integral is expressed as function of exponential-integral functions that are calculated numerically using its series expansion. The mathematical derivation of the solution was performed for two typical heating conditions often encountered in pyrolysis experiments, namely constant temperature and constant heating rate. The sensitivities of the solution with respect to the different model parameters were also calculated.

The analytical solution was illustrated on a six-reaction pyrolysis model for the linearly increasing temperature case. We showed the high accuracy of the proposed analytical solution by comparing it with a numerical solution, and we showed that the computational gain could be significant when performing, for instance, parameter inference compared to the numerical solution.

We finally ended with a local sensitivity analysis and we observed the well-known compensation effect and the relative importance of the mass fraction over the other parameters. However this analysis is only reflecting the local behavior about the nominal parameter values.

In future works, this significant gain in computational time due to the use of the analytical solution will be very helpful for building detailed pyrolysis models with a high number of equations by applying Bayesian inference algorithms to infer the parameter values for uncertainty quantification.

A Computation of derivatives

The computation of derivatives is also required for gradient-informed algorithms to compute the solution of inverse problems. Derivatives are expressed here as a function of temperature and for the linearly increasing temperature case as it will be used in an illustrative example in the next section. The chain rule provides the following results:

$$\frac{\partial \nu_j}{\partial \mathscr{A}_i} = m_0 F_{ij} \left((1-\alpha_i)^{n_i-1} \exp\left\{\frac{-\mathscr{E}_i}{\mathscr{R}T}\right\} \left(n_i \mathscr{A}_i \frac{-\partial \alpha_i}{\partial \mathscr{A}_i} + (1-\alpha_i) \right) \right), \tag{37}$$

$$\begin{aligned} \frac{\partial \alpha_i}{\partial \mathscr{A}_i} = &- \left((1-n_i) \left(-\frac{\mathscr{A}_i T}{\beta} \exp\left\{\frac{-\mathscr{E}_i}{\mathscr{R}T}\right\} - \frac{\mathscr{A}_i}{\beta} \frac{\mathscr{E}_i}{\mathscr{R}} \mathrm{Ei}\left\{\frac{-\mathscr{E}_i}{\mathscr{R}T}\right\} + C_i \right) \right)^{\frac{n_i}{1-n_i}} \dots \\ &\times \left(-\frac{T}{\beta} \exp\left\{\frac{-\mathscr{E}_i}{\mathscr{R}T}\right\} - \frac{\mathscr{E}_i}{\mathscr{R}T} \mathrm{Ei}\left\{\frac{-\mathscr{E}_i}{\mathscr{R}T}\right\} + \frac{\partial C_i}{\partial \mathscr{A}_i} \right), \end{aligned} \tag{38}$$

$$\frac{\partial C_i}{\partial \mathscr{A}_i} = \frac{T_0}{\beta} \exp\left\{\frac{-\mathscr{E}_i}{\mathscr{R}T_0}\right\} + \mathrm{Ei}\left\{\frac{-\mathscr{E}_i}{\mathscr{R}T_0}\right\} \frac{\mathscr{E}_i}{\beta \mathscr{R}}, \tag{39}$$

$$\frac{\partial \nu_j}{\partial \mathscr{E}_i} = m_0 F_{ij} \left((1-\alpha_i)^{n_i-1} \mathscr{A}_i \exp\left\{\frac{-\mathscr{E}_i}{\mathscr{R}T}\right\} \left(n_i \frac{-\partial \alpha_i}{\partial \mathscr{E}_i} - \frac{(1-\alpha_i)}{\mathscr{R}T} \right) \right), \tag{40}$$

$$\begin{aligned} \frac{\partial \alpha_i}{\partial \mathscr{E}_i} = &- \left((1-n_i) \left(-\frac{\mathscr{A}_i}{\beta} T \exp\left\{\frac{-\mathscr{E}_i}{\mathscr{R}T}\right\} - \frac{\mathscr{A}_i}{\beta} \frac{\mathscr{E}_i}{\mathscr{R}} \mathrm{Ei}\left\{\frac{-\mathscr{E}_i}{\mathscr{R}T}\right\} + C_i \right) \right)^{\frac{n_i}{1-n_i}} \dots \\ &\times \left(-\frac{\mathscr{A}_i}{\beta \mathscr{R}} \mathrm{Ei}\left\{\frac{-\mathscr{E}_i}{\mathscr{R}T}\right\} + \frac{\partial C_i}{\partial \mathscr{E}_i} \right), \end{aligned} \tag{41}$$

$$\frac{\partial C_i}{\partial \mathscr{E}_i} = \frac{\mathscr{A}_i}{\beta \mathscr{R}} \mathrm{Ei}\left\{\frac{-\mathscr{E}_i}{\mathscr{R} T_0}\right\}, \tag{42}$$

$$\begin{aligned}\frac{\partial \nu_j}{\partial n_i} =& m_0 F_{ij} A_i \exp\left\{\frac{-\mathscr{E}_i}{\mathscr{R} T}\right\} (1-\alpha_i)^{n_i-1} \dots \\ & \times \left(n_i \frac{-\partial \alpha_i}{\partial n_i} + (1-\alpha_i)\log(1-\alpha_i)\right),\end{aligned} \tag{43}$$

$$\begin{aligned}\frac{\partial \alpha_i}{\partial n_i} =& -\left(((1-n_i)(B_i+C_i))^{\frac{1}{1-n_i}} \dots \right. \\ & \left. \times \left(\frac{-B_i + (1-n_i)\frac{\partial C_i}{\partial n_i} - C_i}{(1-n_i)^2 (B_i+C_i)} + \frac{\log\{(1-n_i)(B_i+C_i)\}}{(1-n_i)^2}\right)\right),\end{aligned} \tag{44}$$

$$\frac{\partial C_i}{\partial n_i} = -\frac{(1-\alpha_0)^{1-n_i}}{(1-n_i)^2} - \frac{(1-\alpha_0)^{1-n_i}\log(1-\alpha_0)}{1-n_i}, \tag{45}$$

$$B_i = -\frac{\mathscr{A}_i}{\beta}\left(T \exp\left\{\frac{-\mathscr{E}_i}{\mathscr{R} T}\right\} + \frac{\mathscr{E}_i}{\mathscr{R}} \mathrm{Ei}\left\{\frac{-\mathscr{E}_i}{\mathscr{R} T}\right\}\right). \tag{46}$$

Note that in Eq. 43, the last term on the right-hand side may pose some numerical issues because of the indetermination. This is the case, for instance, after sufficiently large time after the reaction is completed, or when the different reactants have distant activation energies leading to the reaction i being completed much earlier than other ones. In both cases, $\alpha_i \to 1$ and we have to resolve $(1-\alpha_i)\log(1-\alpha_i)$ for which the limit $0 \times \infty$ is of indeterminate form. This limit can be determined using l'Hôpital's rule for computing the limit of the ratio of two functions and is equal to 0. Practically speaking, in our numerical implementation, every time one of the advancement of reaction factor α_i reaches a value of $\varepsilon_\alpha = 1 - 10^5$, we set to zero the quantity $(1-\alpha_i)\log(1-\alpha_i)$.

Derivatives with respect to F_{ij} are trivial. Issues regarding the computation of the solution when $\alpha_i \to 1$ in $(1-\alpha_i)^{n_i-1}$ with $0 < n_i < 1$ that may arise are avoided because we assumed that $n_i > 1$. Finally, because the pyrolysis reactions are considered to be independent (parallel), we have $\partial\pi/\partial\mathscr{A}_i = \partial\pi_i/\partial\mathscr{A}_i = \partial(\nu_j/\gamma_{ij})/\partial\mathscr{A}_i$ (same for $\mathscr{E}_i$, n_i, F_i).

Acknowledgements The work of J. Coheur is supported by the Fund for Research Training in Industry and Agriculture (FRIA) 1E05418F provided by the Belgian Fund for Scientific Research (F.R.S.-FNRS). The research of F. Torres-Herrador is supported by SB PhD fellowship 1S58718N of the Research Foundation Flanders (FWO).

Conflict of interest

The authors declare that they have no conflict of interest.

References

1. G. Duffa, *Ablative thermal protection systems modeling*. Reston, Virginia: American Institute of Aeronautics and Astronautics, Inc., 2013.

2. S. D. Williams and D. M. Curry, "Thermal protection materials: Thermophysical property data," in *NASA Reference Publication RP-1289*, 1992.
3. M. Stackpoole, S. Sepka, I. Cozmuta, and D. Kontinos, "Post-Flight Evaluation of Stardus Sample Return Capsule Forebody Heatshield Material," *Journal of Thermophysics and Heat Transfer*, vol. 24, no. 4, pp. 694–707, 2010.
4. M. Wright, I. Cozmuta, B. Laub, Y.-K. Chen, and W. H. Wilcoxson, "Defining ablative thermal protection system margins for planetary entry vehicles," in *42nd AIAA Thermophysics Conference*, American Institute of Aeronautics and Astronautics, jun 2011.
5. SpaceX, "PICA-X Heat Shield of Dragon capsule," Apr. 2013.
6. M. Natali, I. Puri, M. Rallini, J. Kenny, and L. Torre, "Ablation modeling of state of the art EPDM based elastomeric heat shielding materials for solid rocket motors," *Computational Materials Science*, vol. 111, pp. 460–480, jan 2016.
7. T. Reimer, C. Zuber, J. Rieser, and T. Rothermel, "Determination of the mechanical properties of the lightweight ablative material zuram," in *Ceramic Transactions Series*, pp. 311–326, John Wiley & Sons, Inc., feb 2018.
8. H.-W. Wong, J. Peck, R. Bonomi, J. Assif, F. Panerai, G. Reinish, J. Lachaud, and N. Mansour, "Quantitative determination of species production from phenol-formaldehyde resin pyrolysis," *Polymer Degradation and Stability*, vol. 112, pp. 122–131, 2015.
9. H.-W. Wong, J. Peck, J. Assif, F. Panerai, J. Lachaud, and N. N. Mansour, "Detailed analysis of species production from the pyrolysis of the phenolic impregnated carbon ablator," *Journal of Analytical and Applied Pyrolysis*, vol. 122, pp. 258–267, nov 2016.
10. B. K. Bessire and T. K. Minton, "Decomposition of phenolic impregnated carbon ablator (PICA) as a function of temperature and heating rate," *ACS Applied Materials & Interfaces*, vol. 9, pp. 21422–21437, jun 2017.
11. F. Torres-Herrador, V. Leroy, B. Helber, L. Contat-Rodrigo, J. Lachaud, and T. Magin, "Multi-component pyrolysis model for thermogravimetricanalysis of phenolic ablators and lignocellulosic biomass," *AIAA Journal*, 2020.
12. A. Martin and I. Boyd, "Strongly coupled computation of material response and nonequilibrium flow for hypersonic ablation," *Journal of Spacecraft and Rockets*, vol. 52, no. 1, pp. 89–104, 2015.
13. J. Lachaud, J. Scoggins, T. Magin, M. Meyer, and N. Mansour, "A generic local thermal equilibrium model for porous reactive materials submitted to high temperatures," *International Journal of Heat and Mass Transfer*, vol. 108, pp. 1406–1417, 2017.
14. P. Schrooyen, K. Hillewaert, T. E. Magin, and P. Chatelain, "Fully Implicit Discontinuous Galerkin Solver to Study Surface and Volume Ablation Competition in Atmospheric Entry Flows," *International Journal of Heat and Mass Transfer*, vol. 103, pp. 108–124, 2016.
15. J. Coheur, A. Turchi, P. Schrooyen, and T. Magin, "Development of a unified model for flow-material interaction applied to porous charring ablators," in *47th AIAA Thermophysics Conference*, (Denver, CO, US), pp. 1–13, American Institute of Aeronautics and Astronautics, jun 2017.
16. F. Torres-Herrador, J. B. Meurisse, F. Panerai, J. Blondeau, J. Lachaud, B. K. Bessire, T. E. Magin, and N. N. Mansour, "A high heating rate pyrolysis model for the phenolic impregnated carbon ablator (PICA) based on mass spectroscopy experiments," *Journal of Analytical and Applied Pyrolysis*, p. 104625, may 2019.
17. F. Torres-Herrador, V. Leroy, B. Helber, L. Contat-Rodrigo, J. Lachaud, and T. Magin, "Multicomponent Pyrolysis Model for Thermogravimetric Analysis of Phenolic Ablators and Lignocellulosic Biomass," *AIAA Journal*, vol. 58, no. 9, pp. 4081–4089, 2020. Publisher: American Institute of Aeronautics and Astronautics _eprint: https://doi.org/10.2514/1.J059423.
18. G. Rein, C. Lautenberger, A. C. Fernandez-Pello, J. L. Torero, and D. L. Urban, "Application of genetic algorithms and thermogravimetry to determine the kinetics of polyurethane foam in smoldering combustion," *Combustion and Flame*, vol. 146, pp. 95–108, July 2006.
19. C. Lautenberger and A. C. Fernandez-Pello, "Optimization Algorithms for Material Pyrolysis Property Estimation," *Fire Safety Science*, vol. 10, pp. 751–764, 2011.
20. D. I. Kolaitis and M. A. Founti, "Development of a solid reaction kinetics gypsum dehydration model appropriate for CFD simulation of gypsum plasterboard wall assemblies exposed to fire," *Fire Safety Journal*, vol. 58, pp. 151–159, may 2013.
21. Q. Nguyen, T. Ngo, P. Tran, P. Mendis, M. Zobec, and L. Aye, "Fire performance of prefabricated modular units using organoclay/glass fibre reinforced polymer composite," *Construction and Building Materials*, vol. 129, pp. 204–215, dec 2016.
22. M. C. Bruns, "Inferring and propagating kinetic parameter uncertainty for condensed phase burning models," *Fire Technology*, vol. 52, pp. 93–120, feb 2015.

23. A. C. Y. Yuen, T. B. Y. Chen, G. H. Yeoh, W. Yang, S. C.-P. Cheung, M. Cook, B. Yu, Q. N. Chan, and H. L. Yip, "Establishing pyrolysis kinetics for the modelling of the flammability and burning characteristics of solid combustible materials," *Journal of Fire Sciences*, vol. 36, pp. 494–517, sep 2018.
24. A. Yuen, T. Chen, C. Wang, W. Wei, I. Kabir, J. Vargas, Q. Chan, S. Kook, and G. Yeoh, "Utilising genetic algorithm to optimise pyrolysis kinetics for fire modelling and characterisation of chitosan/graphene oxide polyurethane composites," *Composites Part B: Engineering*, vol. 182, p. 107619, feb 2020.
25. W. Zhang, J. Zhang, Y. Ding, Q. He, K. Lu, and H. Chen, "Pyrolysis kinetics and reaction mechanism of expandable polystyrene by multiple kinetics methods," *Journal of Cleaner Production*, p. 125042, nov 2020.
26. A. K. Galwey and M. E. Brown, *Thermal Decomposition of Ionic Solids*. Amsterdam: Elsevier, 1999.
27. J. Šesták and G. Berggren, "Study of the kinetics of the mechanism of solid-state reactions at increasing temperatures," *Thermochimica Acta*, vol. 3, pp. 1–12, oct 1971.
28. J. Málek and J. Criado, "Empirical kinetic models in thermal analysis," *Thermochimica Acta*, vol. 203, pp. 25–30, 1992.
29. M. E. Brown, M. Maciejewski, S. Vyazovkin, R. Nomen, J. Sempere, A. Burnham, J. Opfermann, R. Strey, H. L. Anderson, A. Kemmler, R. Keuleers, J. Janssens, H. O. Desseyn, C.-R. Li, T. B. Tang, B. Roduit, J. Málek, and T. Mitsuhashi, "Computational aspects of kinetic analysis. Part A: The ICTAC kinetics project-data, methods and results," *Thermochimica Acta*, vol. 355, pp. 125–143, 2000.
30. C. Di Blasi, "Modeling chemical and physical processes of wood and biomass pyrolysis," *Progress in Energy and Combustion Science*, vol. 34, pp. 47–90, Feb. 2008.
31. S. Vyazovkin, A. K. Burnham, J. M. Criado, L. A. Pérez-Maqueda, C. Popescu, and N. Sbirrazzuoli, "ICTAC kinetics committee recommendations for performing kinetic computations on thermal analysis data," *Thermochimica Acta*, vol. 520, pp. 1–19, jun 2011.
32. J. E. White, W. J. Catallo, and B. L. Legendre, "Biomass pyrolysis kinetics: A comparative critical review with relevant agricultural residue case studies," *Journal of Analytical and Applied Pyrolysis*, vol. 91, pp. 1–33, may 2011.
33. S. Vyazovkin and C. A. Wight, "Model-free and model-fitting approaches to kinetic analysis of isothermal and nonisothermal data," *Thermochimica Acta*, vol. 340-341, pp. 53–68, dec 1999.
34. M. C. Kennedy and A. O'Hagan, "Bayesian calibration of computer models," *Journal of the Royal Statistical Society: Series B (Statistical Methodology)*, vol. 63, pp. 425–464, aug 2001.
35. H. N. Najm, B. J. Debusschere, Y. M. Marzouk, S. Widmer, and O. P. Le Maître, "Uncertainty quantification in chemical systems," *International Journal for Numerical Methods in Engineering*, vol. 80, pp. 789–814, nov 2009.
36. N. Koga, "A review of the mutual dependence of Arrhenius parameters evaluated by the thermoanalytical study of solid-state reactions: the kinetic compensation effect," *Thermochimica Acta*, vol. 244, pp. 1–20, oct 1994.
37. A. K. Burnham and L. N. Dinh, "A comparison of isoconversional and model-fitting approaches to kinetic parameter estimation and application predictions," *Journal of Thermal Analysis and Calorimetry*, vol. 89, pp. 479–490, jul 2007.
38. J. H. Flynn, "The 'temperature integral' — its use and abuse," *Thermochimica Acta*, vol. 300, pp. 83–92, oct 1997.
39. G. I. Senum and R. T. Yang, "Rational approximations of the integral of the arrhenius function," *Journal of Thermal Analysis*, vol. 11, pp. 445–447, jun 1977.
40. J. Farjas and P. Roura, "Isoconversional analysis of solid state transformations," *Journal of Thermal Analysis and Calorimetry*, vol. 105, pp. 757–766, mar 2011.
41. W. Tang, Y. Liu, H. Zhang, and C. Wang, "New approximate formula for arrhenius temperature integral," *Thermochimica Acta*, vol. 408, pp. 39–43, dec 2003.
42. M. Starink, "The determination of activation energy from linear heating rate experiments: a comparison of the accuracy of isoconversion methods," *Thermochimica Acta*, vol. 404, pp. 163–176, sep 2003.
43. C. Deng, J. Cai, and R. Liu, "Kinetic analysis of solid-state reactions: Evaluation of approximations to temperature integral and their applications," *Solid State Sciences*, vol. 11, pp. 1375–1379, aug 2009.
44. S. Vyazovkin, "Modification of the integral isoconversional method to account for variation in the activation energy," *Journal of Computational Chemistry*, vol. 22, no. 2, pp. 178–183, 2000.
45. J. J. M. Órfão, "Review and evaluation of the approximations to the temperature integral," *AIChE Journal*, vol. 53, no. 11, pp. 2905–2915, 2007.

46. J. I. Carrero and A. F. Rojas, "Calculation of the temperature integrals used in the processing of thermogravimetric analysis data," *Ingeniería y competitividad*, vol. 21, pp. 1–10, aug 2019.
47. B. L'vov, *Thermal Decomposition of Solids and Melts*. Springer, english ed., 2007.
48. J. Blondeau and H. Jeanmart, "Biomass pyrolysis at high temperatures: Prediction of gaseous species yields from an anisotropic particle," *Biomass and Bioenergy*, vol. 41, pp. 107–121, 2012.
49. S. Vyazovkin and C. A. Wight, "Kinetics in solids," *Annual Review of Physical Chemistry*, vol. 48, pp. 125–149, oct 1997.
50. H. E. Goldstein, "Pyrolysis Kinetics of Nylon 6-6, Phenolic Resin, and Their Composites," *Journal of Macromolecular Science: Pt. A - Chemistry*, vol. 3, no. 4, pp. 649–673, 1969.
51. K. A. Trick, T. E. Saliba, and S. S. Sandhu, "A kinetic model of the pyrolysis of phenolic resin in a carbon/phenolic composite," *Carbon*, vol. 35, no. 3, pp. 393–401, 1997.
52. L. Torre, J. M. Kenny, and A. M. Maffezzoli, "Degradation behaviour of a composite material for thermal protection systems part I–experimental characterization," *Journal of Materials Science*, vol. 33, pp. 3137–3143, jun 1998.
53. L. Torre, J. M. Kenny, and A. M. Maffezzoli, "Degradation behaviour of a composite material for thermal protection systemsPart II process simulation," *Journal of Materials Science*, vol. 33, pp. 3145–3149, jun 1998.
54. J. L. Clayton, "Thermal/pyrolysis gas flow analysis of carbon phenolic material," in *The Tenth Thermal and Fluids Analysis Workshop*, no. NASA/CP-2001-211141, 2001.
55. A. Bhatia and S. Roy, "Modeling the motion of pyrolysis gas through charring ablating material using discontinuous galerkin finite elements," in *48th AIAA Aerospace Sciences Meeting Including the New Horizons Forum and Aerospace Exposition*, American Institute of Aeronautics and Astronautics, jan 2010.
56. Y.-K. Chen and F. S. Milos, "Effects of nonequilibrium chemistry and darcy—forchheimer pyrolysis flow for charring ablator," *Journal of Spacecraft and Rockets*, vol. 50, pp. 256–269, mar 2013.
57. J. Lachaud and N. N. Mansour, "Porous-material analysis toolbox based on OpenFOAM and applications," *Journal of Thermophysics and Heat Transfer*, vol. 28, no. 2, pp. 191–202, 2014.
58. J. Lachaud, T. van Eekelen, J. B. Scoggins, T. E. Magin, and N. N. Mansour, "Detailed chemical equilibrium model for porous ablative materials," *International Journal of Heat and Mass Transfer*, vol. 90, pp. 1034–1045, 2015.
59. D. Hu, M. Chen, Y. Huang, S. Wei, and X. Zhong, "Evaluation on isothermal pyrolysis characteristics of typical technical solid wastes," *Thermochimica Acta*, vol. 688, p. 178604, jun 2020.
60. K. A. Trick and T. E. Saliba, "Mechanisms of the pyrolysis of phenolic resin in a carbon/phenolic composite," *Carbon*, vol. 33, no. 11, pp. 1509–1515, 1995.
61. A. Olejnik, K. Gosz, and Ł. Piszczyk, "Kinetics of cross-linking processes of fast-curing polyurethane system," *Thermochimica Acta*, vol. 683, p. 178435, jan 2020.
62. M. Abramowitz and I. Stegun, *Handbook of Mathematical Functions: With Formulas, Graphs, and Mathematical Tables*. Applied mathematics series, U.S. Department of Commerce, National Bureau of Standards, 1972.
63. F. T. Herrador, J. Coheur, J. Blondeau, J. Meurisse, F. Panerai, J. Lachaud, T. Magin, and N. N. Mansour, "Comparison between traditional and competitive reaction models for the pyrolysis of high temperature aerospace materials," in *AIAA Aviation 2019 Forum*, American Institute of Aeronautics and Astronautics, jun 2019.
64. K. Ouchi and H. Honda, "Pyrolysis of coal 1. thermal cracking of phenol-formaldehyde resins taken as coal models.," *Fuel*, no. 38, pp. 429–443, 1959.
65. G. F. Sykes, "Decomposition Characteristics of a Char-Forming Phenolic Polymer Used for Ablative Composites," tech. rep., NASA TN D-3810, 1967.
66. F. Torres-Herrador, J. Coheur, F. Panerai, T. E. Magin, M. Arnst, N. N. Mansour, and J. Blondeau, "Competitive kinetic model for the pyrolysis of the phenolic impregnated carbon ablator," *Aerospace Science and Technology*, vol. 100, p. 105784, may 2019.
67. E. Hairer and G. Wanner, "Stiff differential equations solved by radau methods," *Journal of Computational and Applied Mathematics*, vol. 111, pp. 93–111, nov 1999.
68. C. F. Curtiss and J. O. Hirschfelder, "Integration of stiff equations," *Proceedings of the National Academy of Sciences*, vol. 38, pp. 235–243, mar 1952.